

*Society of Plastic Engineers: Automotive Composites Conference & Exhibition
Sept 7–9, Novi, MI*

VALIDATION OF MATERIAL MODELS: DESIGN AND ANALYSIS OF COMPOSITE FRONT BUMPER CRUSH-CAN SYSTEM

Praveen Reddy Pasupuleti

Mark Doroudian

Ramesh Dwarampudi

ESI North America

Anthony M. Coppola, Libby Berger

General Motors

Omar Faruque

Ford Motor Company

James Truskin

FCA USA LLC

Manish Mehta

M-Tech International LLC

Abstract

Usage of composite materials for automotive structural components provides potential weight saving to support the required fuel economy improvements. Nevertheless, many challenges exist in implementing composite designs into high-volume automotive applications, including throughput, part quality, part cost, and the relative immaturity of prediction capabilities during the design phase of composite materials and components. This can limit the weight savings opportunity and can increase the cost of composite components by increasing the amount of material required to meet functional objectives, and reliance on repeated physical testing for validation.

To address industry-wide challenges to obtain lighter weight vehicles, the US Automotive Materials Partnership of Ford, GM and FCA (USAMP) initiated the Validation of Material Models (VMM) project with the support of the US Department of Energy (DOE). The primary project goal was to assess the technical readiness of composite crash simulation technology through efforts demonstrating the virtual design of a front-bumper and crush-can (FBCC) system and the validation of its finite element-based performance prediction. The FBCC system could be validated virtually through a series of high and low speed tests that are indicative of real-world impact events required for vehicle safety certification. While weight saving was an important aspect, the objective of the Design/CAE task on the USAMP's VMM project was to deliver an accurate performance prediction of the FBCC system that met the performance objectives of a baseline steel surrogate design. In this paper the design of composite FBCC is presented first with a series of design tweaks to bond composite components in the absence of weld lines, such as adding front and back crush-can flanges, crush-can side flanges, introducing SMC stiffeners,

modifying SMC stiffeners to create additional plane of bonding, creating drafting angles to assist manufacturing process, and other combinations. The effects of these design changes on the FBCC performance were studied through simulation with some assumptions. The paper then describes about a common methodology utilized in CAE world to build material models from tests to accurately predict crash performance. The simulation results presented in this paper demonstrate how material models calibrated from coupon to components tests can be successfully used to predict full scale FBCC models.

1. Introduction

1.1 Background and Introduction

The objective of this four-year, \$7 million U.S. DOE and USAMP Cooperative Agreement project is to validate and assess the ability of physics-based material models to predict crash performance of automotive primary load-carrying carbon fiber composite structures.^[1] Models evaluated include Automotive Composites Consortium/USAMP-developed models from the University of Michigan (UM) and Northwestern University (NWU), as well as four major commercial crash simulation codes: LS-DYNA, RADIOSS, VPS (formerly called PAM-CRASH), and Abaqus. Predictions are presently being compared to experimental results from quasi-static testing and dynamic crash testing of a lightweight carbon fiber composite front-bumper and crush-can (FBCC) system which was selected for demonstration via design, analysis, fabrication, and crash testing. The successful validation of these crash models will facilitate improved design of lightweight carbon fiber composites in automotive structures for mass reductions.

The usage of composites in the automotive industry is widely known, but to realize the effective performance of these composite structures under various load conditions potentially requires many crash tests. To avoid expensive trials, computer-aided engineering (CAE) simulations are used to reduce the number of trial and error procedures in developing a product.

In the past, many researchers have worked on developing numerical models that predicts progressive damage and failure in fiber reinforced laminates [2, 7-8]. In this paper, such commercially available models were used with an attempt to design a composite FBCC within the steel packaging space that is mass producible, production feasible, predictable as steel with equivalent energy absorption to a steel FBCC.

The reliability of these computer-based simulations is greatly dependent on individual crash codes and underlying material models, as well as on the designer's ability to obtain required test data and apply the correct model parameters – all of these factors are highly experience-based and require strong knowledge of composite materials and computational methods. Different CAE codes have different test property and data requirements but a minimum common set of material tests across all codes is sufficient to run initial simulations. However, the accuracy and predictability of simulations often relates to how well the tests were controlled and performed, repeatability and the ability to produce all the required tests.

The first step in developing the composite FBCC was to establish design targets based on a steel FBCC system. The existing steel FBCC was initially simulated under various crash loads to generate target energy absorption requirements. The steel FBCC simulations from CAE codes correlated reasonably well with experiments. Once the design targets were set for an equivalent composite FBCC, an iterative process via simulations was executed to optimize the composite design to fit within the set design space. Multiple iterations were conducted to optimize the shape of the components, evaluate competing manufacturing processes, type of material, layup sequence, attachment methods, etc. The material models selected for crash analysis were validated against simple tension, compression and shear properties, although

different tests were required to address the unique characterization requirements of the some of the newer material model codes. While two different materials (unidirectional (UD) and woven) laminates were tested and simulated, only woven composites were selected by the USAMP team for the design of the composite FBCC. Following coupon and component level validations, a full FBCC crash analysis under 6 different load conditions was executed. Key metrics being used to compare CAE to tests include: force versus deflection response, average crush force, crush distance, acceleration versus time response, and displacement versus time response and composite failure mechanisms.

The design also had a weight save target of >30 percent less than the steel FBCC. Unlike a steel assembly, the attachment of composite crush-cans to composite bumper cannot be performed via traditional welding or riveting techniques, and required a unique joining strategy to implement localized bonding on critical interfaces. A novel, patent-pending strategy was adopted to mold SMC backing plate material onto the rear end of crush-cans in order to effectively attach the full FBCC to the crash sled utilizing bolts. This paper describes the process for establishing design targets for the composite FBCC, achieving a manufacturable design of composite FBCC and developing predictions from VPS crash code.

2. Design Targets

The selected baseline steel FBCC design donated by Ford shown in Figure 1 was simulated under various load conditions (4 high speed and 2 low speed) using four different commercial codes i.e., (VPS, LS-DYNA, RADIOSS and Abaqus). The material data for different steel sub-components was supplied by Ford and is highlighted in Table 1. VPS MAT 103 Elastic-Plastic Iterative Hill was used for all deformable steel components. The provided plastic behavior for bumper and crush-can is shown in Figure 2 and 3. Strain rate dependency was only modeled for crush-cans, Figure 3. Material and spot weld failure were not considered in the models. A series of high speed and low speed impact simulations were carried out in VPS as shown in Table 2.

Table 3 illustrates the key design targets for composite FBCC as derived from Steel FBCC predictions, which were collaboratively established by the VMM Project Design/CAE Team, comprised of a multi-disciplinary technical staff, in order to leverage critical mechanics, materials, processing, joining and NDE expertise amongst OEMs, suppliers and academics.

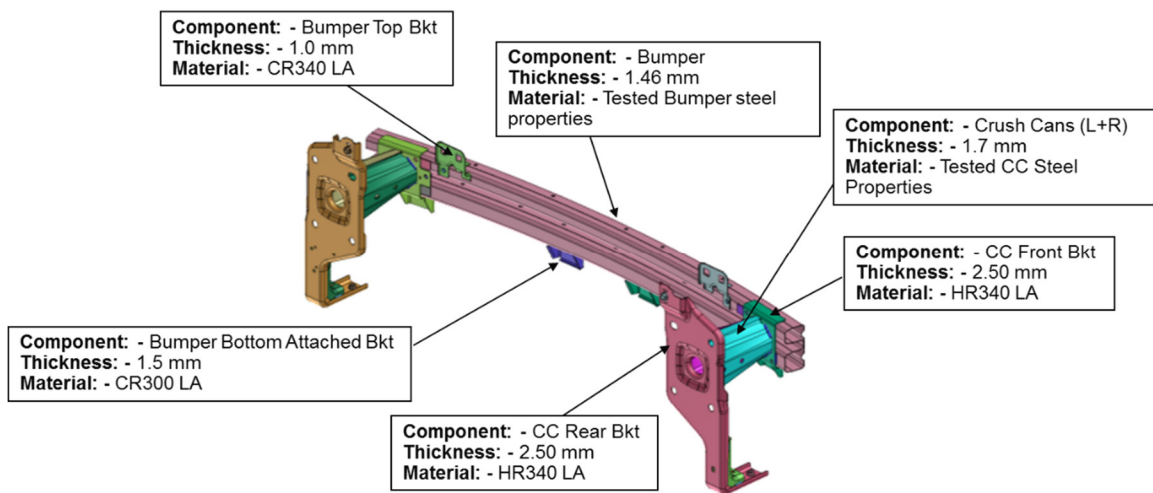


Figure 1. Steel FBCC Components

Table 1. Material Properties of Steel FBCC Components

(* Plastic material properties)

Material	Density (kg/mm ³)	Elastic Modulus (GPa)	Poisson's Ratio	Yield Strength (GPa)	UTS (GPa)	% elongation at yield
CR300 LA	7.80E-06	210	0.3	0.3	0.42	26
CR340 LA	7.80E-06	210	0.3	0.34	0.45	23
HR340LA	7.80E-06	210	0.3	0.34	0.45	22
Tested Bumper steel	7.80E-06	210	0.3	*	*	*
Tested Crush Can (CC) steel	7.80E-06	210	0.3	*	*	*

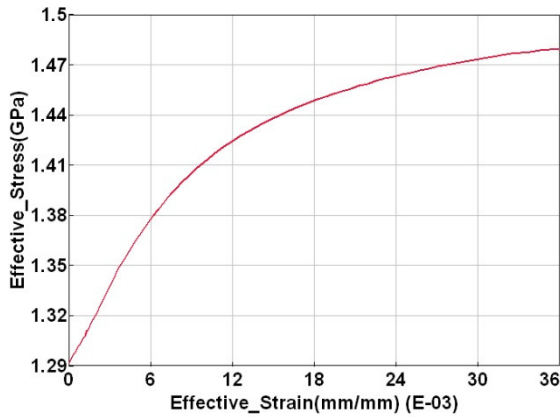


Figure 2. True Stress-Strain for Steel Bumper

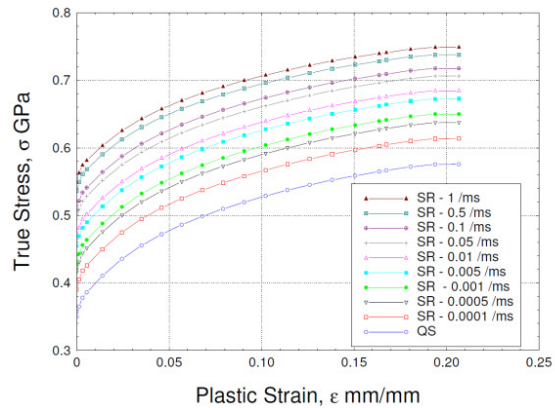


Figure 3. Rate Dependent True Stress-Strain Curve for Crush-Cans

Table 2. High Speed and Low Speed Test Conditions for Steel FBCC

No.	Load Case	Mass (kg)	Speed (mph)
1	Rigid Full (NCAP)	300	35
2	Rigid Offset	321.34	26.54
3	Rigid Angular (30 Degree)	321.34	20.29
4	Rigid Center Pole	306	14.35
5	Pendulum Impact Center	302.3	10.05
6	Pendulum Impact Quarter	326.4	9.5

Table 3. Design Targets for Composite FBCC Design

No.	Load Case	Energy Absorption, EA (kJ)	Average Crush Force (kN)	Crush Distance (mm)
1	Rigid Full (NCAP)	37	220	200
2	Rigid Offset	22	120	200
3	Rigid Angular (30 Degree)	13	90	150
4	Rigid Center Pole	6	N/A	N/A
5	Pendulum Impact Center	3	N/A	N/A
6	Pendulum Impact Quarter	3	N/A	N/A

3. Design of Composite FBCC

Over twenty conceptual designs were discussed for the composite front bumper and crush-can system along with material systems and manufacturing processes during the initial phase of the project. A final design for composite FBCC was selected as shown in Figure 4. The design consists of a C-Channel bumper beam section with chopped carbon fiber SMC ribs (to retain rigidity) and a two-piece crush-can with embedded SMC base. To ease NDE (Non-Destructive Evaluation) inspection, crush-cans with flat facets (instead of round or conical shape) were chosen.

The materials and processing systems (MPS) team selected “compression molding” as a primary method to mold composite FBCC components, after initially examining thermoforming and pultrusion for uniform crush-can cross-sections. The key consideration was that compression molded parts can be produced at a high rate which is one of the key requirements for mass applications of composites in the U.S. automotive industry.

Several details were considered in the design of the FBCC. One key design iteration for the bumper involved the design of the front bumper flanges, as shown in Figures 5-6. It is expected that a bumper will tend to first bend backward and then flex back after any frontal impact. A simulation study, conducted by ESI, concluded that the bumper with flanges performed better than without flanges under certain load conditions. The reverse curl in the bumper flanges (shown in Figure 5) brings the neutral axis to approximately the center of the cross-section and creates equal strains on the front and rear where strain levels are at their maximum.

Another key design iteration for the bumper was the inclusion of a compression molded back-plate, shown in Figure 6. Simulations carried out on FBCC models with back plate proved beneficial for concentrated loads such as pole impacts. Without a back-plate, the force induced by the pole is concentrated locally and cause the bumper material to fail (Figure 7) before the load is transferred to the crush-cans. To avoid such failure, a back plate was modeled and bonded to the flanges of the bumper using. The predictions show that a bumper with back-plate helps distribute the concentrated load throughout the Beam (Figure 8). However, the additional piece and assembly cost of the back-plate, combined with the additional weight led the team to decide to not include this piece in the final FBCC proposal, as it did not add significant value to the objective of correlating the material models, although it did improve performance.

SMC ribs (Chopped Carbon Fiber) co-molded inside the C-channel bumper were designed to increase flexural rigidity of the bumper and avoid opening of the bumper during crash loads. The SMC ribs were also used to position and constrain the two crush-cans in an adhesive joint with the bumper (as shown in Figure 1).

Different crush-can shapes and reinforcement concepts were considered but a two-piece, conical dodecagonal face crush-can design was eventually selected, which best balanced performance, NDE and manufacturing objectives (Figure 9-10). Flanges on either side of each crush-can were designed to provide bond interface surfaces. Stand-offs were molded into the flanges to maintain a consistent bond-line of 1.0 mm thickness, shown in Figures 11 and 12. Stand-offs were shaped such that the lower flange with 31° depressions will allow upper flange with 30° cone to register on the round end. Holes on crush-can side flanges (Figures 9 and 10) represent rivet locations used to bond crush-can halves in addition to adhesive applied on flat surfaces; whereas, holes on rear flange of the crush-can represent bolt locations used to join the complete FBCC assembly to the back rail of the sled. Crush-can halves are molded to form circular flanges on the front end which will be used as bonding surfaces with the bumper beam (Figure 13). A second plane of bonding is provided via the SMC rib shown in Figure 14. Stand-offs were designed on the external surfaces of SMC ribs to facilitate ease of bonding.

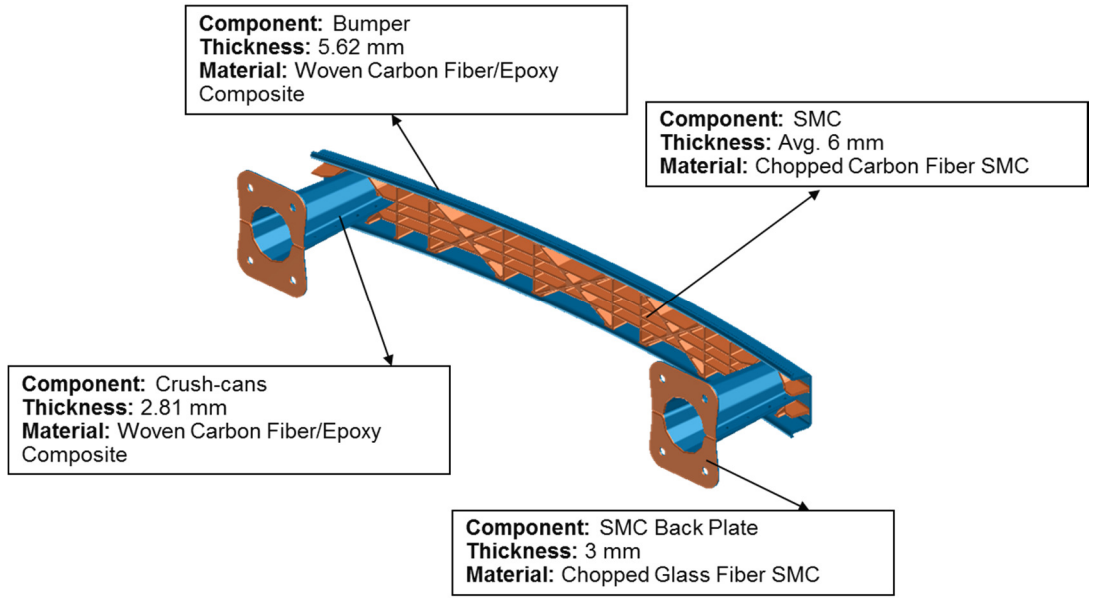


Figure 4. Composite FBCC Design and Material Strategy

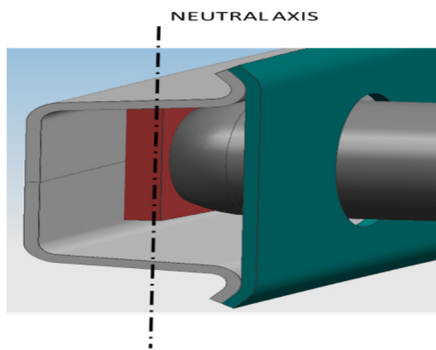


Figure 5. Bumper with Flanges

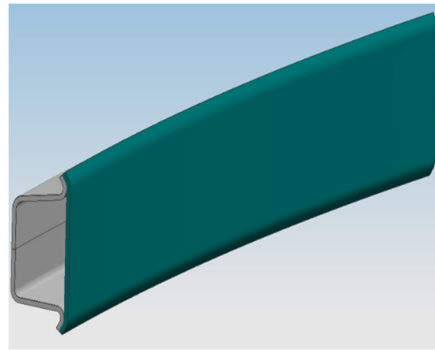


Figure 6. Bumper with Back-Plate

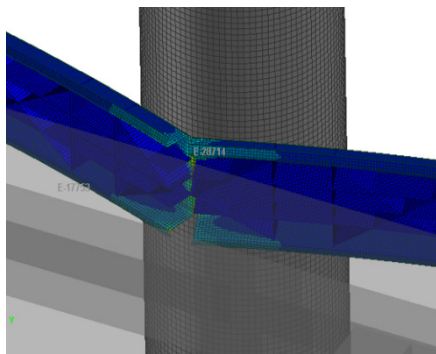


Figure 7. Bumper without Back-Plate

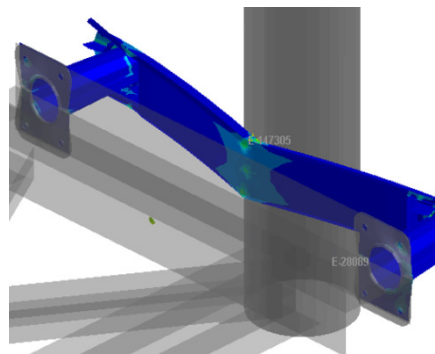


Figure 8. Bumper with Back-Plate

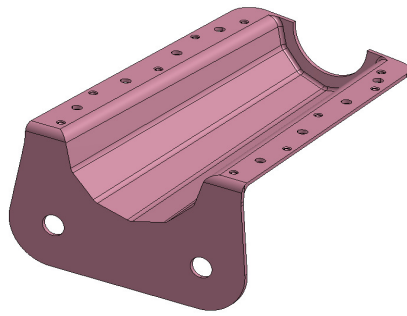


Figure 9. Can Upper Half

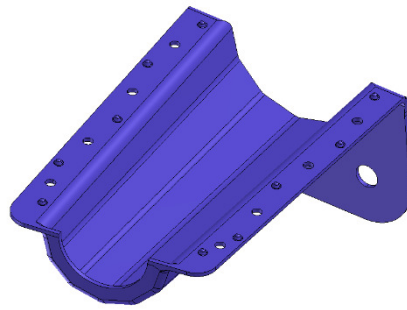


Figure 10. Can Lower Half



Figure 11. Stand-Off on Upper Half



Figure 12. Standoff Receiver on Lower Half

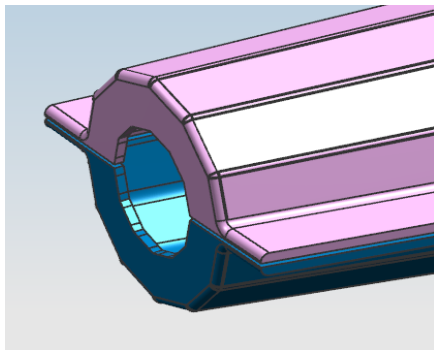


Figure 13. Front End Flange

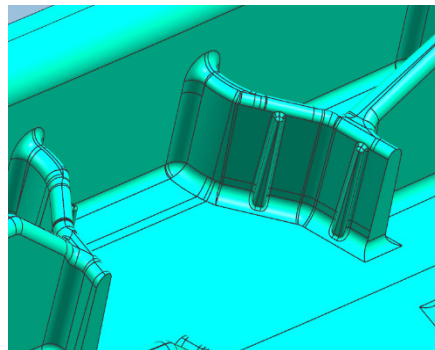


Figure 14. Standoffs on SMC

As shown in Figures 15 and 16, both crush-cans and bumper were designed to have at least 25 mm run-off extension to avoid resin rich areas while matching the actual CAD.

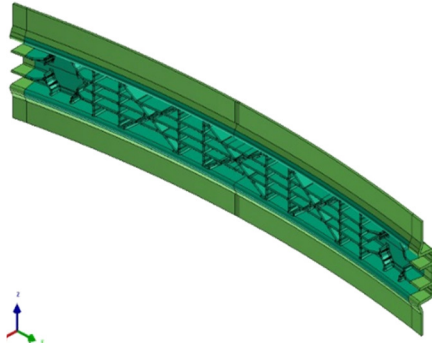


Figure 15. Bumper with Extension

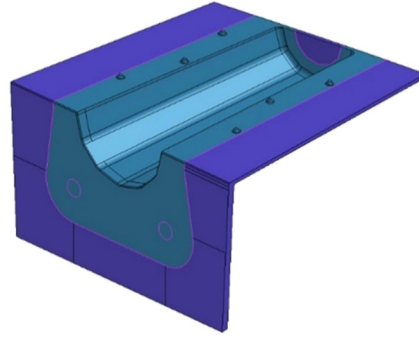


Figure 16. Crush-Can with Extension

4. Finite Element Model

The explicit dynamic finite element code VPS was used with the continuous damage mechanics model MAT 132 to predict the crash performance of the composite FBCC under 6 different load cases as outlined in Table 2.

4.1 Model Development

The finite element model (FEM) for composite parts was developed using 3/4 node shell elements with one integration point per layer. Figure 17 shows the FEM. The sled was modeled as a rigid body with a point mass of 300 kg at the center of gravity. A target element size of 3.0 mm was imposed to all composite components. A friction coefficient value of 0.3 was used between the wall and the FBCC assembly. The contact between the impactor (wall) and the composite parts was defined using “Symmetric Node-to-Segment with Edge Treatment” card definition in VPS. The contact force generated between impactor and the composite parts was monitored using a penalty option. The total solution time for the 70 milliseconds NCAP crash event took about 15 hours to solve using VPS 2015.0 on a 12 CPU workstation.

The SMC ribs inside the bumper are constructed with 3 and 4 node shell elements. The SMC at the rear crush-can was modeled using 8 node brick elements. The crush-cans designs consist of 12 layers of woven carbon fiber with epoxy and the layup for the bumper is a 24-layer woven carbon fiber with epoxy. Table 4 shows individual components with laminate information. The number of plies and sequence chosen was based on optimization studies that met performance criteria under axial, angular and static loads. The model assumes that for every 0-layer there is a 90-degree layer, and properties in both directions are identical. Delamination between two adjacent layers was not modeled, as a single shell with multi-layers was used to represent laminate, and to keep the modeling strategy same across all four commercial codes.

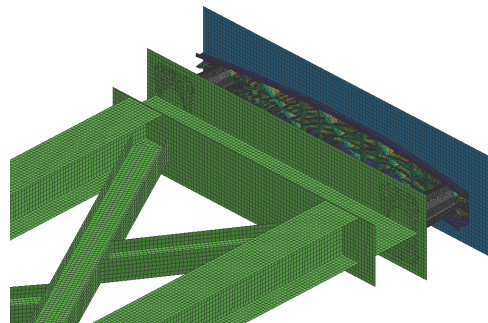


Figure 17. FE Model Illustration for NCAP

Table 4. Composite Layup/Thickness

No.	Component	Layup	Thickness (mm)
1	Bumper	$[0/45/-45/90/90/-45/45/0]_{2s}$	5.62
2	Crush-Can	$[0/45/-45/90/45/0]_s$	2.8
3	SMC at Bumper	N/A	6
4	SMC at Crush-Can	N/A	3

4.2 Connections, Contact and Boundary Conditions

Unlike the steel FBCC, the joints requiring weld lines or spot welds are to be replaced by adhesive in the case of the composite FBCC. In the FE models, adhesive was modeled as 1D tied bar elements with no failure considered, this is again kept same across all four commercial codes being evaluated. The crush-can front section is tied to the bumper and SMC ribs through 1D bar elements (Figure 20-21). Chopped carbon fiber SMC ribs are integrally molded into the bumper (Figure 22). In FE models, the ribs-to-bumper connection was modeled as coincident node-to-node connection with no failure considered at the interface. Glass fiber SMC used at the rear of the crush-can was modeled as solid elements and the interface between carbon fiber crush-can and glass fiber SMC was represented by 1D bar elements with no interface failure.

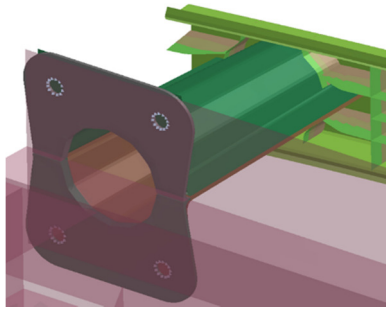


Figure 18. Bolts Connecting Crush-Can to Sled are represented via 1D Tied Elements

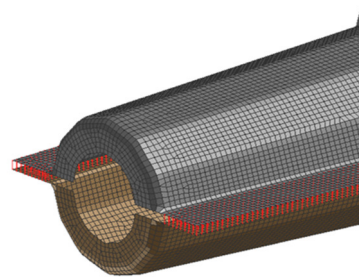


Figure 19. Crush-Can Side Flange Bonding represented with 1D Tied Elements

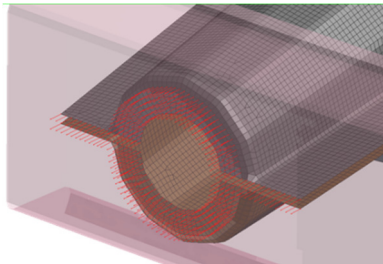


Figure 20. Front CAN-Bumper Tied Link

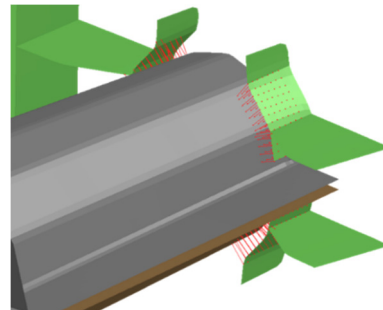


Figure 21. CAN-SMC Tied Link

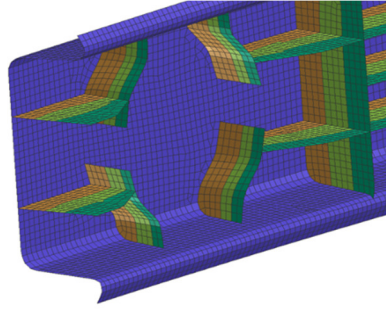


Figure 22. SMC-Bumper Node-to-Node Connection

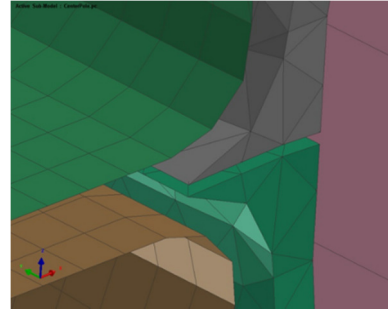


Figure 23. SMC-Crush Can Tied Link

4.3 Material Models and Properties

All rigid bodies were modeled using MAT 100 (*Linear Elastic Null Material) with the properties of steel (Table 5). A continuous damage mechanics model, MAT 131 (*Multi-Layered Orthotropic Bi-Phase) in VPS has been used to model the progressive damage behavior of carbon fiber/epoxy woven composites. The material properties and parameters of MAT 131 are presented in Table 6.

MAT 131 is a multi-layered composite shell element material model with ply types 1 & 2 used for global ply damage law. Ply type-1 is intended for uni-directional composites (shell elements) but can also be used to approximate woven fabric by stacking two UD layers with appropriate fiber angles and distribution of mechanical properties (Table 7). For the project, Ply Type-1 was used to represent Woven fabric composites.

Ply model TYPE-1 is based on research by P. Ladevèze and E. Ledantec and is modified to include transverse shear by A. Hurez.^[1] It corresponds to a homogenized, global description of the fiber and matrix phases. The fiber phase uses a strain-based failure criteria for tension and compression. Non-linear (elastic) behavior is possible in compression and is often necessary to account for micro-buckling effects in compression. The shear behavior uses a coupled damage and plasticity model that accounts for modulus reduction and permanent plastic deformations.

Further details on the MAT 131 model can be found in the MAT 131 of VPS User Manual [3]. MAT 105 (* Elastic-Plastic ITR with ISO Damage) was used to define SMC chopped carbon fibers for ribs in the bumper with properties shown in Table 8. MAT 01 (*Elastic-Plastic Solid) was used to define SMC chopped fibers located at the rear of Crush-Can with properties as illustrated in Table 9.

Table 5. Elastic Properties of Steel

*MAT	ρ , kg/m ³	E, GPa	ν
100 (*Null Material Shell)	7.85E-06	210	0.3

Table 6. Material Properties and Parameters of MAT 131

ITYP	RHO	E0t1	E0t2	NU12	
1	1.48E-06	1	101.6	0.055	Elasticity
G012	G023	G012	E0c1	GAMMA	
9.3	4.74	4.74	102.6	0	Damage
EPSifti	EPSiftu	Dftu	IFUND1	ISHD	
0.0108	0.0308	0.9	2	2	
EPSifci	EPSifcu	Dfcu			Plasticity
0.0129	0.0329	0.9			
R0	BETA	m			Strain Rate
0.028	1.21	0.4446			
ERATER11	D11	n11	D11r	n11r	Failure Model
-	-	-	-	-	
FAILDAM	FAILTYP	EPSIslim			
1	0	0.15			

Table 7. Ply Types 1 & 2 in MAT 131^[5]

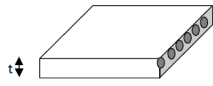
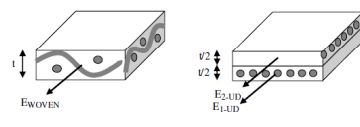
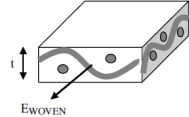
Option / Ply type	Representation	Comments
1 (Ply type 1)		Standard representation for UD composite plies
2 (Two layers of Ply type 1)		<ul style="list-style-type: none"> The woven composite is idealised as two stacked plied of ply type 1 In plane and shear properties must be carefully distributed between plies Useful for non-orthogonal reinforcement and large shear loading
3 (Ply type 7)		<p>Standard representation for woven composite plies:</p> <ul style="list-style-type: none"> Ideally for orthogonal reinforcement Intra-ply shear strains should not be large

Table 8. SMC Properties for Chopped Carbon Fiber Composites (Shell)

*MAT	ρ , kg/m ³	G, GPa	ν
105 (*Elastic-Plastic-ITR- with ISO Damage)	1.39E-06	10.47	0.45
SIGM-OPTN	SIGMAy	K, GPa	
Yield Stress	0.16	101.26	
EPSIpmax			
0.015			

Table 9. SMC Properties for Chopped Carbon Fiber Composites (Solids)

*MAT	ρ , kg/m ³	G, GPa	K, GPa
01 (*Elastic-Plastic-Solid)	1.39E-06	10.47	101.26
SIGM-OPTN	SIGMAy		
Yield Stress	0.16		

5 Material Model Validation

A single-element and coupon-level simulations were carried out in VPS to calibrate MAT 131 described above. Coupon tests were performed by Delsen Test Laboratories (now known as Delsen division of Element) on two different material systems, UD and Woven Carbon Fiber/Epoxy systems. Additionally, component level (Hat-Plate) calibrations were also carried out in VPS to further validate MAT 131. Hat-Plate axial crush tests were conducted by team members at the University of Michigan.

5.1 Single Element and Coupon Calibration of MAT 131

The necessary material properties for stiffness and failure were extracted from standardized tests. The model and input data were then validated using a single element and coupon test case as shown in Figure 24.

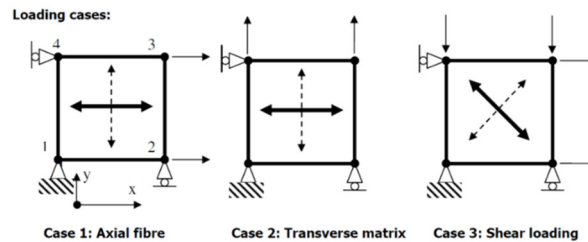


Figure 24. A Single Element Description of FE Model

5.1.1 Tension Test

The element was loaded at a constant velocity of 1.0 mm/ms. Five coupons were loaded in the 0° tension direction (=90° direction for a balanced woven fabric composite). Good correlation was found for stiffness and failure data as summarized in Table 10 and Figure 25.

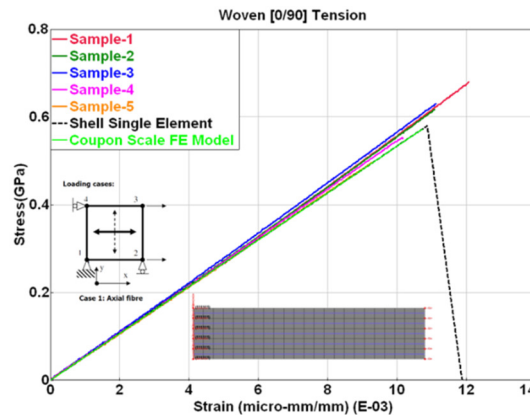


Figure 25. Fiber Tension in [0]° Direction

Table 10. Property Extraction from Test Data for 0° Tension Fiber Direction

Property	Value
E_1^{0t} Tensile Elastic Modulus (Fiber Direction)	50.8 GPa (101.6 GPa for Ply-1)
σ_i^{ft} Tensile Failure Stress (Fiber Direction)	580 MPa
ν_{12} Poisson's Ratio	0.055
ϵ_i^{ft} Tensile Failure Strain (Fiber Direction)-Initiation	0.0108
ϵ_u^{ft} Tensile Failure Strain (Fiber Direction)-Ultimate	0.0109
d_u^{ft} Assumed Ultimate Damage (Fiber Direction)	0.9

5.1.2 Compression Test

Coupons were also loaded in the 0° direction compression (=90° direction for a balanced woven fabric composite). Some scatter was observed in the test data (Figure 26) but reasonable averages for stiffness and failure data were found as summarized in Table 11.

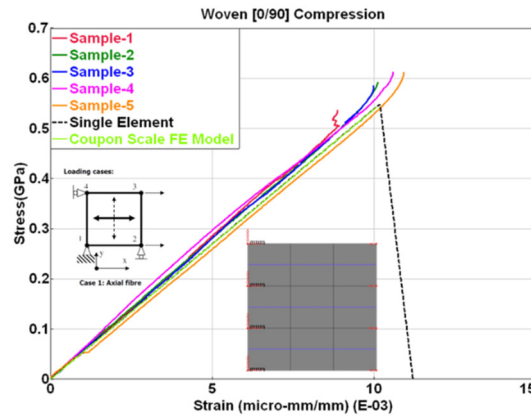


Figure 26. Fiber Compression in [0]° Direction

Table 11. Property Extraction from Test Data for 0° Compression Fiber Direction

Property	Value
E_1^{0c} Compression Elastic Modulus (Fiber Direction)	51.3 GPa (102.6 GPa for Ply-1)
σ_i^{fc} Compression Failure Stress (Fiber Direction)	619 MPa
ϵ_i^{fc} Compression Failure Strain (Fiber Direction)-Initiation	0.0129
ϵ_u^{fc} Compression Failure Strain (Fiber Direction)-Ultimate	0.0130
d_u^{fc} Assumed Ultimate Damage (Fiber Direction)	0.9

5.1.3 Shear Test

To capture the shear behavior for woven composites, +/- 45° coupons were cyclically loaded with cycles of 10% ultimate tensile strain (17%, 25%, 37.5%, 50%, 70% and 90%) to get at least five damage points. The average ultimate tensile strain of 1.08% was obtained from 0° degree tension test. The cyclic test was used to extract damage evolution, plasticity and final shear strain data. G_{12}^0 is given by the initial slope of the shear stress (σ_{12}) versus the engineering shear strain ($2 \epsilon_{12}$) curve.

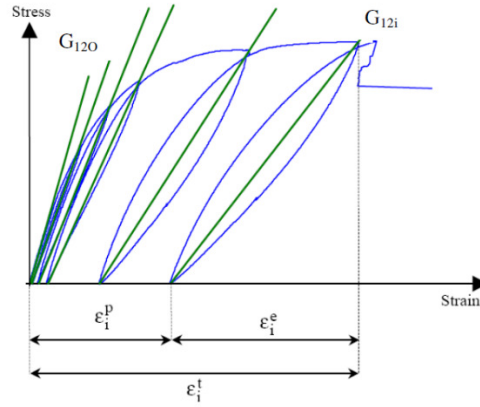


Figure 27. Shear Response via Cyclic Curve (Schematic)^[5]

Shear damage is given by the change in slope of the cyclic modulus G_{12}^i with each loading cycle (i). Initial slope of the un-damaged cyclic stress-strain curve gives the initial shear modulus. At each cycle, stiffness loss is characterized by modulus reduction. The degree of shear damage d_{12} is given by the relationship in Equation-1.

$$d_{12}^i = 1 - \left(\frac{G_{12}^i}{G_{12}^0} \right) \quad (1)$$

The model uses the term Y_{12} to define damage progression given by relation (Equation-2).

$$Y_{12}^i = \sqrt{\frac{1}{2} G_{12}^0 (2\varepsilon_{12}^e)^2} \quad (2)$$

From the cyclic curve and above expressions, it is possible to plot the evolution of Y_{12} damage d_{12} for each loading cycle (i), as shown in Table 12.

Table 12. Shear Elastic Damage Evolution

Cycle	G_{12} (GPa)	$(2\varepsilon_{12}^e)$	d_{12}	Y_{12}
0	9.37	0.00306	0	0
1	8.06	0.00488	0	0.006
2	7.21	0.00771	0.235	0.015
3	6.62	0.01027	0.357	0.022
4	5.64	0.01381	0.423	0.028
5	4.57	0.01620	0.457	0.032
6	4.28	0.01884	0.492	0.038

Plasticity is given by the growth of plastic strains (ε_{12}^p). The model uses the term (p_i) as a measure of effective plastic strain. The term (R_i) is used to evaluate influence of damage (d_{12}) to yield stress (R_0) in each loading cycle.

$$p_i = \int_{\varepsilon_{12}^{p_{i-1}}}^{\varepsilon_{12}^{p_i}} 2(1 - d_i) \varepsilon_{12}^p \quad (3)$$

$$P_j = \sum_{i=1}^{i=j} p_i \quad (4)$$

$$R_i = \frac{\sigma_{12}^i}{1 - d_i} - R_o \quad (5)$$

Finally, a curve fitting exercise was performed to fit exponential plasticity function (with parameters β and m) to the R_i versus p_i curve, Equation-6.

$$R_i = \beta(P_j)^m \quad (6)$$

Table 13 summarizes plasticity results obtained from the integration and summation equations 3 to 6. A good correlation has been found between test and simulation (Figure 28).

Table 13. Shear Plasticity Behavior for Woven Carbon Fiber/Epoxy Composites

Cycle	$(2\varepsilon_{12}^p)$	$(1-d_{12})$	p_i	p_j	R_i
0	0	1	0	0	0
1	0.00019	0.8994	0.000185	0.000185	0.012529
2	0.00087	0.7911	0.000525	0.000710	0.026603
3	0.00221	0.7160	0.000903	0.001614	0.044446
4	0.00471	0.5918	0.001504	0.003118	0.054344
5	0.00856	0.4552	0.001782	0.004900	0.061865
6	0.01328	0.4177	0.001960	0.006861	0.062844

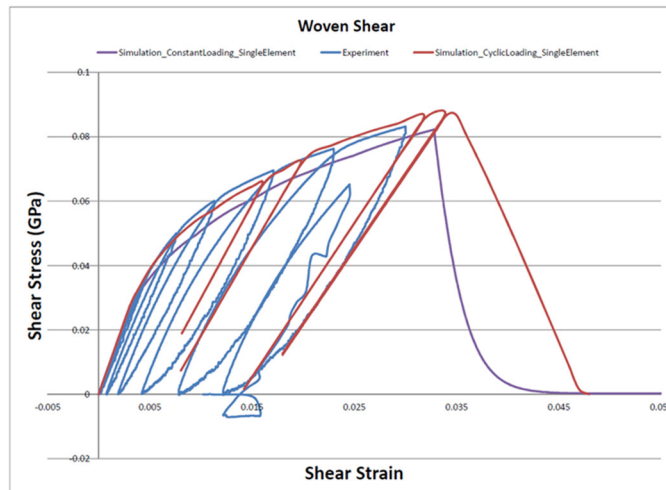


Figure 28. Shear Behavior of Woven Carbon/Epoxy Composites

5.2 Hat-Plate Calibration of MAT 131

A Hat-Plate design of three different ply configurations (Table 14) was tested in crush loading. The dimensions of the component are shown in Figure 30. The plate was bonded to a hat section on the side flanges using epoxy adhesive from Dow (BETAMATE® 73326/73327). An aluminum block was manufactured with a slot to fit the bottom 25 mm of the part; and a plastic epoxy putty was used to bond the part in the slot (Figure 30).

An Instron Dynatup Impact test machine (Figure 29) was used to crush samples. A mass of 74.5 Kg was dropped from a height of 0.98 meters. Table 14 shows test results for different ply configurations and the corresponding VPS simulation results. The force-deflection overlays of test and VPS simulations are shown in Figures 31-33. Both, in experiments and simulations, it was observed that crush initiates on the front and proceeds rear; however, simulations show large peaks of force during crush followed by instantaneous drop of force. This is a typical behavior in CAE models characterized by the sudden deletion of elements until next rows of elements are in contact. This sudden deletion of elements could be attributed to hard contact between the impact plate and the hat-plate composite model, or due to other numerical effect; this behavior could be further investigated. Figures 31-33 reveals a high frequency noise in the CAE (un-filtered) data than the test data. When plotted against SAE Class 180 filter, it not only smoothens out high frequency signals but also follow closely peaks and valleys of the original CAE signal. An acceptable correlation to test was obtained in terms of the total crush length and the average crush force for QI and Cross-Ply Woven laminates, however, some discrepancy was found for UD/Woven combo laminates.

Table 14. Axial Crush Test vs Predictions

	QI Woven				0/90 Woven					UD/Woven QI			
Layup for Hat Section	[0/90/45/-45/0/90/0/-45/45/90/0] - 11 Layers				[0/90/0/90/0/90/0/90/0/90/0] - 11 Layers					[0/0/0/90/45/90/-45/90/0/0/0] - 11 Layers			
Layup for Plate	[0/90/45/-45/0/90/0/-45/45/90/0] - 11 Layers				[0/90/0/90] _s - 8 Layers					[0/90/45/-45/0/90/0/-45/45/90/0] - 11 Layers			
Specimen ID	S-1	S-2	Test Avg.	VPS	S-3	S-4	S-5	Avg.	VPS	S-6	S-7	Avg.	VPS
Crush Distance, mm (Test)	18.2	15.5	16.85	15.8	14.5	16.2	17.7	16.13	17.5	20.1	16.3	18.2	15.3
Plateau Load, kN (Test)	41	41	41	44	36	-	36	36	35	35	35	35	50

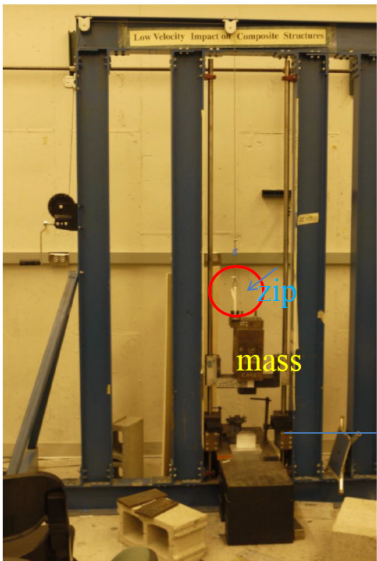


Figure 29. Test Equipment

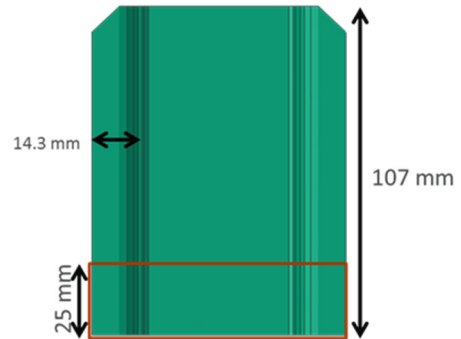
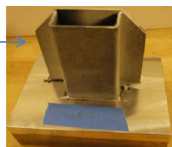
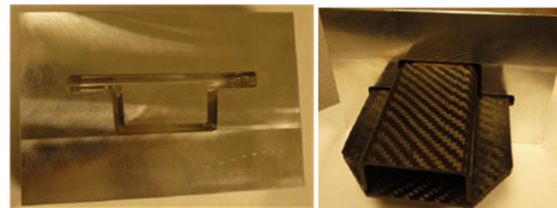


Figure 30. Hat-Plate



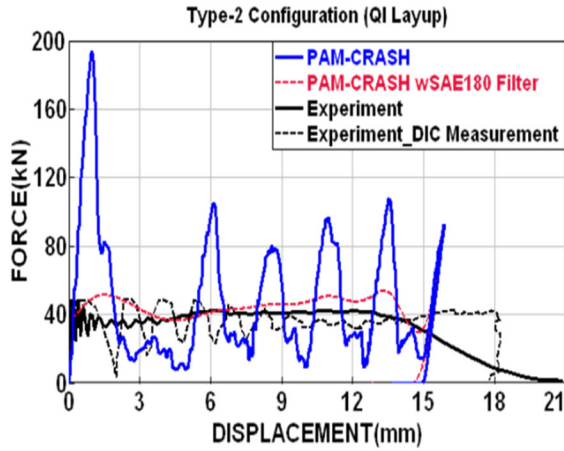


Figure 31. Quasi-Isotropic Woven Laminate

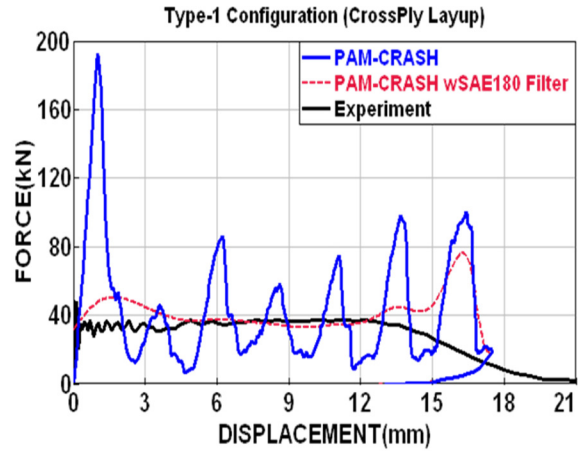


Figure 32. Cross-Ply [0/90] Woven Laminate

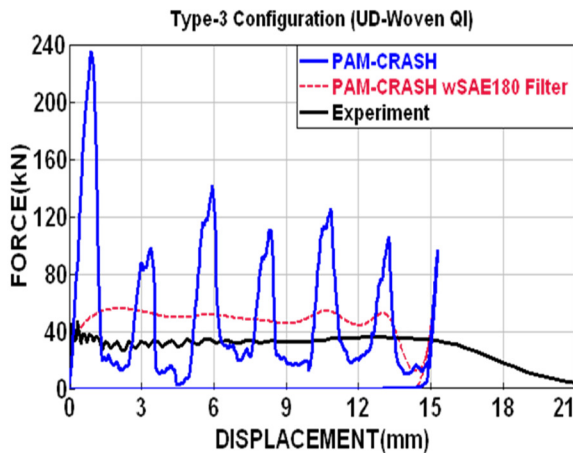


Figure 33. UD/Woven Laminate

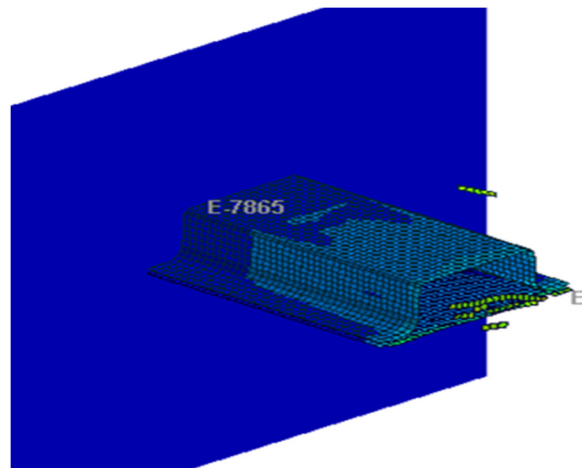


Figure 34. VPS Simulation

6 Composite Full FBCC Crash Simulations

The contact force versus displacement response between wall/impactor and the composite FBCC for each load case are presented in Figure 35-40. Overlays of VPS predictions for the steel FBCC and composite FBCC for the same boundary and initial conditions are also presented.

For composites, the initial velocity for the Center-Pole impact load case has been reduced by half in order to withstand complete energy absorption. Unlike steel which undergoes energy absorption via plastic deformation due to its ductile nature, composites absorb a significant amount of energy through cracking and breaking by due to their brittleness. This phenomenon, was especially evident for the center-pole impact at 14 mph. For composites, there is no “folding deformation” which generally occurs in steel; once a ply fails, elements need to be eroded in order to maintain numerical stability, and the next rows of elements engage in contact; this is evident from the force-deflection curves where element deletion results in a sudden force drop.

The trend in steel and composites behavior is similar where the force increases to peak from the initial impact up to flexing of the Bumper, followed by stable crushing/folding of crush-cans. A complete energy absorption (EA) for both steel and composites was achieved for the same given kinetic energy. The equivalent energy absorption for composites was achieved at a mass savings of nearly 40% as shown in Table 16. Table 15 shows steel and composites FBCC predictions under various load scenarios.

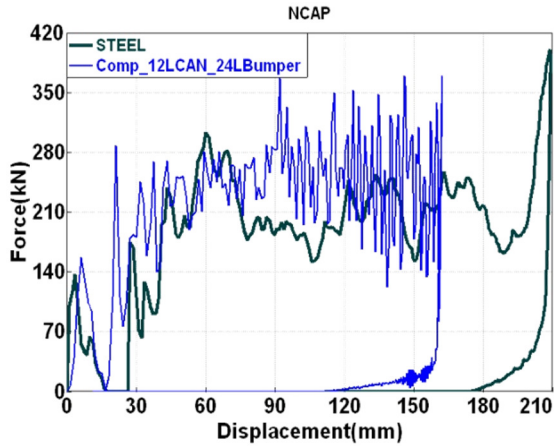


Figure 35. NCAP

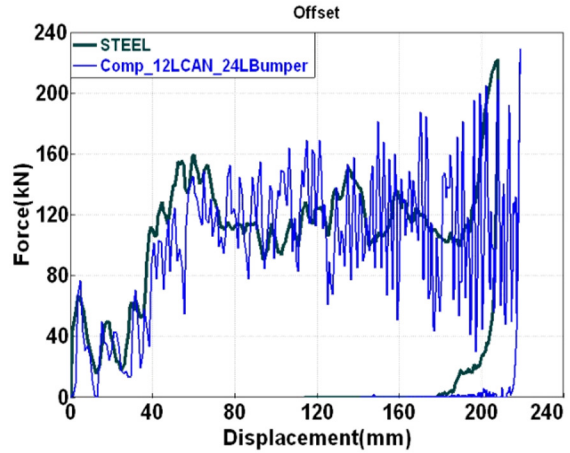


Figure 36. Offset

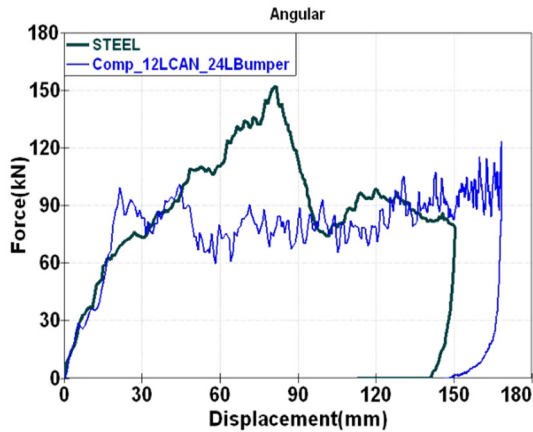


Figure 37. Angular

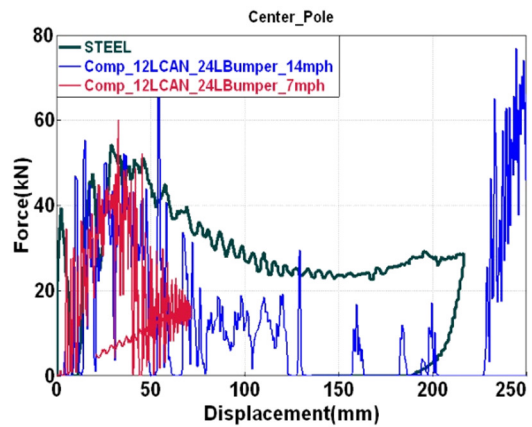


Figure 38. Center-Pole

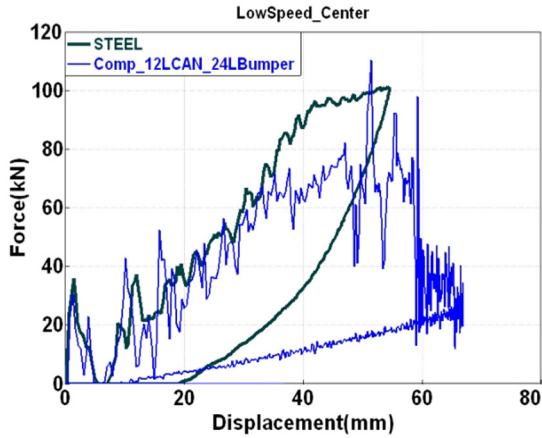


Figure 39. Pendulum Impact-Center

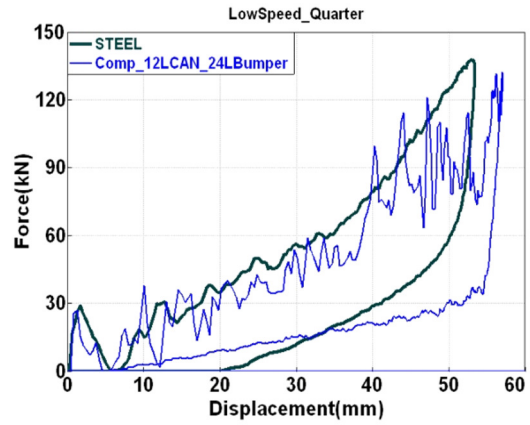


Figure 40. Pendulum Impact-Quarter

Table 15. Steel FBCC vs Composite FBCC Predictions

No.	Load Case	STEEL FBCC Simulations			Composite FBCC Simulations		
		Energy Absorption, EA (kJ)	Average Crush Force (kN)	Crush Distance (mm)	Energy Absorption, EA (kJ)	Average Crush Force (kN)	Crush Distance (mm)
1	NCAP	36	220	200	35	250	162
2	Offset	22	120	200	22	120	218
3	Angular	13	90	150	13.2	88	165
4	Center Pole	5	N/A	N/A	3	N/A	N/A
5	Pendulum Impact Center	3	N/A	N/A	2	N/A	N/A
6	Pendulum Impact Quarter	3	N/A	N/A	2	N/A	N/A

Table 16. Mass Comparison between Steel FBCC and Composite FBCC

Component	Total Mass (Kg)
STEEL	
Steel Bumper	5.27
Steel Crush-Cans	1.84
Front Bracket	0.93
4 Additional Bumper Attachments	0.26
Rear Bracket	2.7
2 Additional Rear Bracket Attachments	0.29
Total Mass	11.29
Total Mass Without Additional Attachments	10.74
COMPOSITE	
Bumper 24 Layers	2.76
Crush-Cans 12 Layers	1.0
SMC Ribs in Bumper (7-5 mm Thick)	1.88
SMC Rear (~ 3 mm Thick)	0.21
Total Mass	5.85
Mass Savings Over Steel	48.18%
Mass Savings Without Additional Attachments	45.53%

Manufacturing defects (e.g., fiber misalignment, micro-voids, wrinkles, thickening/thinning, resin-rich areas, etc.) could have a significant influence on the crash performance of structural composite parts. To produce accurate predictions, it is recommended that FE models consider manufacturing defects, which are often the source of unpredicted and premature failure, as they influence the manner in which damage is developed and evolved through the impact event. The behavior must be better characterized in order to provide more accurate predictions.

Other tools exist, such as PAM-FORM and Fibersim which can be used to consider ply mechanical data, process conditions and other factors which can be input into the CAE model to improve the discrete characterization of individual elements in the model to consider processing effects and better account for induced instabilities in the design from the manufacturing process [9]. While this activity was conducted, it is not in the scope of this paper.

7 Conclusions

Significant progress has been made towards the design and development of composite models for assessing FBCC performance under various crash loads. Finite element modeling was used to guide the development of composite FBCC models from establishing design targets to characterizing material models using the state of the art material models. The finite element models captured experimental coupon and component behavior quite well, though some adjustment of model parameters may still be needed. A good correlation to experiments on the coupon level and component level suggests that full FBCC predictions created using this method can efficiently assess the crash behavior under different load conditions, however, assumptions like no delamination and no failure in the models need to be verified. To further improve the models, the effects of manufacturing-induced defects and fiber orientation changes should be considered.

8 References

1. Ladevèze P, Le Dantec E, "Damage Modelling of the elementary ply for laminated composites", *Composites. Science and Technology*, Vol. 43, Issue 3, 1992, pp. 257-267.
2. A.K. Johnson, A.K. Pickett and P. Rozycki, "*Computational methods for predicting impact damage in composite structures*", *Composites Science and Technology*, Vol-61 (15), pp. 2183-2192, 2001; concluding Reference [2].
3. VPS (Virtual Performance Solution) Solver Reference Manual, ESI Group, Vol1-6, Version 2015.0.
4. PAM-QUICKFORM User Guide-Solver, ESI Group, Version 2011.
5. A.K. Pickett, "Composite Global Ply Model 131 for Elastic, Damage and Failure", ESI GmbH/Institute for Aircraft Design, Stuttgart, September 2012.
6. A.K. Pickett, "Impact and Crash Simulation of Composite Materials-Training", ESI GmbH, Eschborn, Germany, March 2009.
7. V.Klesher, R.Zemick, T.Kroupa, "Identification and Verification of the Composite Material Parameters for the Ladeveze Damage Model", University of West Bohemia in Pilsen, Department of Mechanics, Czech Republic, April 2011.\
8. E.J.Pineda, A.M.Waas,"Numerical Implementation of a Multiple-ISV Thermodynamically Based Work Potential Theory for Modeling Progressive Damage and Failure in Fiber-Reinforced Laminates, December 2011.
9. C.C. Chou, J.Le, P.Chen, D.J. Bauch, "Development of CAE Simulated Crash Pulses for Airbag Sensor Algorithm/Calibration in Frontal Impacts", Ford Motor Company, Research and Vehicle Technology, U.S.A. 301.
10. X.Jin, "US-3 Validation of Material Models: Composite Fabric Manufacturing Studies by Simulation and Experiment", SPE-Automotive Composite Conference, Novi, MI 2016.

Acknowledgements

This program is supported by the U.S. Department of Energy under Cooperative Agreement Number DE-EE0005661 awarded to the United States Automotive Materials Partnership. Neither the United States Government nor any agency thereof, nor any of their employees, make any warranty, express or implied, or assumes any legal liability or responsibility for the accuracy, completeness, or usefulness of any information, apparatus, product, or process disclosed, or represents that its use would not infringe privately owned rights. Reference herein to any specific commercial product, process, or service by trade name, trademark, manufacturer, or otherwise does not necessarily constitute or imply its endorsement, recommendation, or favoring by the United States Government or any agency thereof. The views and opinions of authors expressed herein do not necessarily state or reflect those of the United States Government or any agency thereof.